Nonlocal and Light Cone Dynamics Emergent from Information-Propagating Complete Graph

Thomas L. Wood
Unconventional Computing
University of the West of England

Theories relating to the discretization of spacetime and results from quantum information theory have indicated that physically observable behavior may be emergent from such an underlying yet unknown microscopic theory. In this paper, a candidate discrete system based on the structure presented in [1] is explored via direct computational implementation. The microstates of the system evolve via information transfer mechanisms on dynamic complete graphs built upon substitution networks developed in [1]. Using the positive integer edge weights as measures of distance, the system is artificially embedded in $\mathbb{R}^n$ by treating the flat space violations as stress, resulting in a curved geometry (Figure 1). This stress then effects a force on the vertices. In this paper, light cone dynamics of the motion of the minima of this stress are observed, along with superluminal motion of the vertices. We argue that this superluminal velocity corresponds to the quantum mechanical discontinuous motion of particles and provides possibilities for descriptions of entanglement and particle spin within the system. Further to this, that the compatibility of this type of dynamics with relativistic behavior makes this system nontrivial and worthy of further investigation.

Keywords: point particle; interaction edge; space element; state graph; duplication; reduction; microstate; stress minimization; embedding; cumulative velocity; minimized velocity

1. Introduction

The notion that observed physical behaviors are emergent from a *bottom-up* microscopic description has been incorporated in various areas of theoretical physics in recent years. Causal set theory describes an abstract generalized structure of such a description [2, 3]. Recent insights from holography and quantum information theory [4–6], as well as other new theoretical insights [7, 8], also imply an underlying microscopic description. In other words, quantum mechanics tells us a lot about how likely something is to happen, but it does not tell us why, on the most fundamental level, it is that likely to happen. The

https://doi.org/10.25088/ComplexSystems.27.2.127

approach of this paper is motivated by this, along with two reductionist world views. First, that an underlying discrete spacetime structure [9–12] rectifies many of the infinities resulting from the incompatibilities of general relativity and quantum field theory. This is detailed by Sorkin in [13]. The second is that complex dynamics and behaviors emerge from fundamentally simple rules that may be implemented as networks, or cellular automata, on a (quantum) computer [14–18]. In this way, it is not unreasonable to propose that all observable phenomena in the universe may be emergent from a single definable and computable microscopic discrete description of spacetime.

Developments in quantum mechanics suggest that quantum field theory (QFT) may be computable in the form of quantum cellular automata (QCA) [19, 20]. This has led to research such as that of D'Ariano, showing physics as emergent from information processing [21]; essentially that QCA, given the specific fundamental axioms of unitarity, homogeneity, locality and isotropy, can produce QFT as an emergent theory [22–24]. The research of Requardt and Rastgoo into the structurally dynamic cellular network followed a somewhat similar approach. Again, the motivation being that underlying spacetime could be adequately described by cellular networks. This research was initiated in the late 1990s with [25] and [26], and continued with some more recent publications [27]. Parallel to this, a similar approach was taken up by Konopka, Markopoulou and Smolin in [28], where they suggest evidence for holography and the black hole entropy law resulting from the continuum spacetime structure emergent from networks, bearing correlations to the later work of Verlinde [5, 6], but in the context of dynamic networks.

In this paper, a microscopic description of such a system is presented, as well as results of physically comparable behavior emergent from its implementation. The system is a development based on the globally interacting fully connected stochastic substitution (FCSS) system presented in [1].

The greatest challenge in describing such a microscopic theory is that it must be consistent with all observation on all energy levels. Therefore, as each layer of detail is added to the description, further consistencies must be realized. The correct microscopic theory should in essence speak for itself, as all physically comparable behavior should be emergent and should ideally be based on rules that are as simple as possible. This paper will attempt to make the case that the rules for the system investigated are indeed nontrivial, while also simple and aesthetic. In Section 4, comparisons with physical systems, parallels to relevant physical theories and suggestions of further areas to investigate in this system are made. So far, apparent physically comparable behavior includes an origin of particle mass, internal particle spin, quantum observation and wave/particle duality, light cone

dynamics and propagation of light/information at the speed of light, variety of interparticle interactions causing the emergence of complex structures, and two possibilities for nonlocal entanglement dynamics and quantum tunneling. These will be explained in more detail in Section 4.

A microscopic description must be Lorentz covariant, something that has proven difficult for many microscopic discrete systems [29]. The system implemented in this paper has a defined spacetime, coordinate bases defined by choosing orientation vertices [1] and a mechanism for transforming between them. In this context, the rules outlined in this paper are consistent with the postulates of special relativity [30]. This is because two metrics are defined, that of the microstate graph and that of the embedded space $\mathbb{R}^n$, and information propagates along the edges of the microstate graph, the geometry of which is independent of the configuration in $\mathbb{R}^n$; therefore, no matter how an observer moves through the system, the rate of information transfer remains constant within the state graph. What we see in this paper is that this rate of information transfer results in light cone dynamics of particles, with the light cones defined on the metric of the system in $\mathbb{R}^n$. Relativity is a local theory and is at odds with quantum entanglement, a nonlocal theory [31]. However, by implementing an information transport mechanism within the discrete system, similar to that implemented in [32], and a hidden velocity variable on vertices, we observe a compatibility of nonlocal action at a distance and local light cone dynamics emergent from the fundamental rules and structure of the system.

It is important to note that this paper is describing a candidate microscopic structure from which physically comparable behavior is expected to be entirely emergent. Therefore, the main aim is to provide a definition of the system along with some preliminary results, with the hopes of stimulating further analysis and investigation of the system. We also hope to help encourage criticism outlining significant violations of physical law that may be faced by this system and others like it.

2. Microstate Description and Rules

A microstate in this system is represented by a complete graph $G = (V, E)$ called the *state graph*, where the vertices represent *point particles* (PPs) and the edge weights represent a measure of spatial extent between PPs called *interaction edges* (IEs). The IEs are chains of indivisible identical cells called *space elements* (SEs). The edge weights of the graph correspond to the number of SEs in each IE that

https://doi.org/10.25088/ComplexSystems.27.2.127

the system is aware of in that moment in time. The graph evolves in discrete clock time, with each constituent (PP, SE) undergoing transition rules through each time step (TS).

2.1 Complete Graph Structure and Transition Rules

During a transition $t \to t+1$, SEs and PPs both have two mutually exclusive probabilistic *actions* that they may undergo.

Every SE within the system may *duplicate* ($1SE \to 2SE$) or *reduce* ($1SE \to 0SE$) with a probability of p_d and p_r, respectively.

Every PP may *split* into two PPs separated by one SE ($1PP \to 2PP + 1SE$) or *merge* all SEs between two PPs reducing in the same TS ($2PP + kSE \to 1PP$), with probabilities p_s and p_r^k, respectively, where k is the number of SEs between the two PPs at time t. In this paper, we are analyzing purely the effect of the information propagation; therefore, we consider the system where $p_s = 0$. If all SEs in an IE reduce in the same TS, then they are replaced by 1 SE.

One PP in this graph is named the *central PP*. At the point in time t that these actions occur, the information of the actions begins to propagate through the IEs at a rate of one SE/TS. A duplication propagates a $+1$ and a reduction propagates a -1; these values undergo superposition as they propagate through the dynamic IEs. This happens on the radial IEs (IEs incident to the central PP) in one direction toward the central PP, and on the nonradial IEs in both directions toward the two enclosing PPs. Information traveling along nonradial IEs is transferred to a radial IE incident to the PP it is propagating toward once it reaches it. This information resides on the gaps (or nodes) between SEs, and so it is stored as integer values in nonradial IEs and as lists of integers in radial IEs. The state of the system updates according to the information that reaches the central PP at any given time slice t. (This results in the fundamental principle of conservation of information. This can be used to check the correctness of coding used to implement the system.) This gives the vertices the role of the observer in the system, much as described by Illachinski [14]. (In this case, propagation would have to be considered as occurring in all directions, as this would force an equivalence between radial and nonradial IEs under a transformation of reference frame/central PP.) This means that there is a global symmetry regarding transformations between vertices within the system's microstates.

There are two representations for the microstates, the *observed microstate* representation (the information that the system is aware of at any time t) and the *hidden microstate* representation (all the information that characterizes the microstate and therefore the corresponding paths).

An observed microstate γ_t takes the form of the state matrix E_t, where $E_t = \{e_{ij}\}_t \in M_{m_t}(\mathbb{N})$, where m_t is the number of PPs at time t, $e_{ij} \in \mathbb{N}$ with $e_{1i} = e_{i1}$, and $e_{ii} = 0$. E_t is a matrix describing the edge weights of graph $G = (V, E)$.

γ_t with γ'_t represents the components of a specific microstate at time t for observed and hidden microstates, respectively. The observed microstate corresponds to $\gamma_t = E_t$, and the hidden microstate γ'_t takes the form of a quadruplet $\gamma'_t = \{E_t, S_t, T_t, R_t\}$. S_t represents the instantaneous number of SEs within the IEs at time t, where $S_t = \{s_{ij}\}_t \in M_{m_t}(\mathbb{N})$, $s_{ij} \in \mathbb{N}$ with $s_{ij} = s_{ji}$ and $s_{ii} = 0$. T_t and R_t represent arrays that store the information of propagating actions within the nonradial and radial IEs in the state graph, respectively. In our case, the number of PPs in the system is kept constant and multiedges are not implemented, so these arrays take the form $T_t = \{\tau_{ij}\}_t$ with $\tau_{ij} \in \mathbb{Z}^{s_{(i+1)(j+1)}+1}$ and $\tau_{ij,k} \in \mathbb{Z}$, and $R_t = \{\rho_i\}_t$ with $\rho_i \in \mathbb{Z}^{s_{1i}+1} \times \mathbb{Z}^{m_t}$ and $\rho_{i,kj} \in \mathbb{Z}$. Both $\tau_{ij,k}$ and $\rho_{i,kj}$ represent the propagating action information on an individual SE.

The action propagation mechanism undergoes the following rules:

1. First, when an SE undergoes an action, that information is initially stored at the boundaries of that SE in the direction of propagation.
   - *i.* If at time $t \to t+1$ SE k in radial IE ρ_i *duplicates*, then $\{\rho'_{i,k1}\}_t = \{\rho_{i,k1}\}_t + 1$, and if it *reduces*, $\{\rho'_{i,k1}\}_t = \{\rho_{i,k1}\}_t - 1$, else $\{\rho'_{i,k1}\}_t = \{\rho_{i,k1}\}_t$.
   - *ii.* If at time $t \to t+1$ SE k in non-radial IE τ_{ij} *duplicates*, then $\{\tau'_{ij,k}\}_t = \{\tau_{ij,k}\}_t + 1$, and if it *reduces*, $\{\tau'_{ij,k}\}_t = \{\tau_{ij,k}\}_t - 1$, else $\{\tau'_{ij,k}\}_t = \{\tau_{ij,k}\}_t$.
2. The location of the information stored within the IE is changed each TS due to the actions that occurred within the IE in that TS. Reductions result in superposition of information. $\{\Delta\alpha^{\rho}_{i,k}\}_t$ and $\{\Delta\alpha^{\tau}_{ij,k}\}_t$ represent the sum of all actions ahead of point k in the direction of propagation at time $t \to t+1$ for radial and nonradial IE, respectively. Duplication adds 1 and reductions subtract 1 from this total. Starting with null arrays, the following procedure is performed for all values of k, starting with 1 and going up to $\{s_{ij}\}_t$:
   - *i.* $\left\{\rho''_{i,(k+\{\Delta\alpha^{\rho}_{i,k}\}_t)j}\right\}_t = \left\{\rho''_{i,(k+\{\Delta\alpha^{\rho}_{i,k}\}_t)j}\right\}_t + \{\rho'_{i,kj}\}_t$.
   - *ii.* $\left\{\tau''_{ij,(k+\{\Delta\alpha^{\tau}_{ij,k}\}_t)}\right\}_t = \left\{\tau''_{ij,(k+\{\Delta\alpha^{\tau}_{ij,k}\}_t)}\right\}_t + \{\tau'_{ij,k}\}_t$.

https://doi.org/10.25088/ComplexSystems.27.2.127

3. The PPs then transfer the nonradial information incident to them into radial information toward the central PP, and the central PP updates its state due to the incident information on it. Then all information does a single propagation to its neighbor in the direction of propagation.
   i. The information incident on each PP is transferred from nonradial to radial, $\left\{\rho_{i,(\{s_{ij}\}_{t+1})(j+1)}\right\}_{t+1} = \{\tau_{ij,1}\}_{t+1}$, and the observed microstate is updated at the central PP, $\{e_{ij}\}_{t+1} = \{e_{ij}\}_t + \{\rho_{i,1j}\}_{t+1}$.
   ii. Then the system does a single SE propagation $\{\rho_{i,k1}\}_{t+1} = \left\{\rho''_{i,(k+1)1}\right\}_t$ and $\{\tau_{ij,k}\}_{t+1} = \left\{\tau''_{ij,(k+1)}\right\}$.

2.2 Stress Minimization Embedding and Forces in $\mathbb{R}^n$

Each microstate path of $\gamma_{t_1} \to \gamma_{t_2}$ is written as $\omega(\gamma_{t_1}, \gamma_{t_2}) \in \varpi(\gamma_{t_1}, \gamma_{t_2})$, where $\omega(\gamma_{t_1}, \gamma_{t_2}) = \{\gamma_{t_1}, \gamma_{t_1+1}, \ldots, \gamma_{t_2-1}, \gamma_{t_2}\}$. This is then mapped by Θ to a path in configuration space $\chi(t_{t_1}, t_{t_2}) = \{X_{t_1}, X_{t_1+1}, \ldots, X_{t_2}\}$, where $X_t = \{x_i\}_t = \{x_0, x_1, \ldots, x_{m_t}\}_t$ with $x_i \in \mathbb{R}^n$. From this, we define $V_t = \{v_i\}_t = \{v_0, v_1, \ldots, v_{m_t}\}_t$ with $v_i \in \mathbb{R}^n$ and $v_{it} = x_{i(t+1)} - x_{it}$, and $A_t = \{a_i\}_t = \{a_0, a_1, \ldots, a_{m_t}\}_t$ with $a_i \in \mathbb{R}^n$ and $a_{it} = v_{it} - v_{i(t-1)}$, where x_{it}, v_{it} and a_{it} are instantaneous positions, velocities and accelerations in spacetime, respectively. (This mathematical representation treats the number of PPs (m_t) in the system as constant, and therefore there is no shifting of the array index due to splitting and merging in this system representation. In implementation, this ideal system can be modeled by putting $p_s = 0$ and enforcing that if $\{s_{ij}\}_t \to 0$, then an instantaneous split occurs to counteract the merger; this is what we have implemented for the purposes of this paper.) For any initial observed microstate E_t there may be multiple paths in configuration space; however, for a specific X_{t_1}, it seems much more likely that only a unique path is mapped to. $e_{ijt} = \{e_{ij}\}_t$, $x_{it} = \{x_i\}_t$, $v_{it} = \{v_i\}_t$ and $a_{it} = \{a_i\}_t$.

The microstate is embedded in $\mathbb{R}^n$ by the map $\Theta : M_{m_t}(\mathbb{N}) \to (\mathbb{R}^n)^{m_t}$, defined as $\Theta(E_{t+1}, X_t, V_t) = (X_{t+1}, V_{t+1})$. The function uses the vector total intrinsic stress incident on each PP, due to the Euclidean violations of the system's configuration in $\mathbb{R}^n$, to constitute an instantaneous acceleration on each PP's velocity at time t:

$$a_{it} = \sum_{i \in \{0, m_t\}} \left(e_{ijt} - \|x_{it} - x_{jt}\|\right) \left[\frac{(x_{it} - x_{jt})}{\|x_{it} - x_{jt}\|}\right]. \tag{1}$$

Equation (1) gives the instantaneous acceleration on a single PP i at time t. Therefore, the following conversions of the coordinates hold at each time step, $v_{jt} = v_{j(t-1)} + a_{jt}$ and $x_{j(t+1)} = x_{jt} + v_{jt}$. This is known as a PP's *cumulative velocity*.

This stress-induced instantaneous acceleration constitutes the dynamics of the positions of the PPs within the system. The acceleration is always directed along stress-minimizing paths toward a local minimum of the stress:

$$[x_{it}]_n = [x_{it}]_{n-1} + \sum_{i \in \{0,\, m_t\}} \left(e_{ijt} - \left\|[x_{it}]_{n-1} - [x_{jt}]_{n-1}\right\|\right) \left[\frac{\left([x_{it}]_{n-1} - [x_{jt}]_{n-1}\right)}{\left\|[x_{it}]_{n-1} - [x_{jt}]_{n-1}\right\|}\right]. \tag{2}$$

Equation (2) describes the iterative formula that relaxes all PPs into a stress-minimizing configuration in $\mathbb{R}^n$. $\tilde{X}_t(X_t)$ is the local minimum for X_t, where $X_t = \{[x_i]_0\}_t$ and $\tilde{X}_t(X_t) = \left\{\left\{\lim_{n\to\infty} [x_i]_n\right\}_t\right\}$. Every microstate has a corresponding geometry, with geodesics that tend toward the local minima. (A sample of these geometries from randomly generated microstates of edge weights between 1 and 100 can be seen in Figure 1.) The velocity of a particle's local stress minimum is known as its *minimized velocity*. In this paper, we give evidence that the minimized velocity of a particle averaged over microstates is bounded to be below 1 SE/TS.

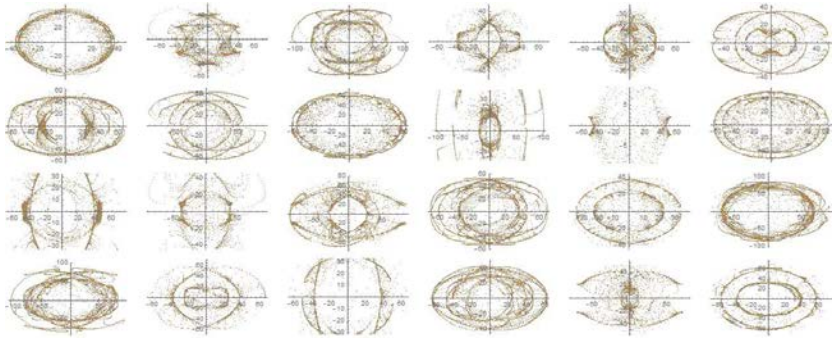

Figure 1. Each image in this figure shows a characteristic geometry that emerges out of an *observed microstate* E_t's embedding in $\mathbb{R}^2$. Each image in the figure corresponds to a system consisting of 4 PPs. The images are formed by plotting the paths taken by 100 samples of $\{X_{n=0}\}_t$, with $n \to 100$. The paths tend toward local minima $\tilde{X}_t(X_t)$ of the stress. Since the state matrix is constant for each geometry, these images represent a snapshot of what the geometry of the state graph embedded in R^2 is at a moment in time.

https://doi.org/10.25088/ComplexSystems.27.2.127

In Section 3, evidence will be provided of how the information propagation rate of one SE per TS within the discrete graph G induces an intrinsic speed limit on the expected velocity of motion of these minima of one SE per TS in $\mathbb{R}^n$. The velocity of PPs in the microstate is cumulative, and therefore maybe far greater than this; however, the direction of acceleration is always along a geodesic directed toward the local minima. The result is a system that contains light cone dynamics of a minimal potential, yet has superluminal oscillatory dynamics that may have deeper correlations to action at a given distance entanglement dynamic of the quantum mechanical wavefunction.

3. Results

An observation is a subset of microstates that satisfy a given condition. This represents the collapse of the macrostate evolution into a specific microstate or set of microstates, much like the collapse of the wavefunction under observation. Therefore, an observation could be characterized as a set of microstates of which one PP exists within a specific region Δx of $\mathbb{R}^n$, much like in a position measurement. The TS after the moment of measurement, there exists a distribution of expected minimized velocities $\langle \tilde{V}_t \rangle$, as well as for the expected cumulative velocities of the PP $\langle V_t \rangle$. Expected velocities are calculated by taking the statistical average of all minimized or cumulative velocities in the instantaneous TS between two sets of microstates.

Figures 2 and 3 show how the mean, standard deviation and maximum values for these distributions change as the size of the sample of microstate paths is increased.

As you can see from Figures 2 and 3, the maximum value for the minimized velocities moves well below 1 when the number of samples is increased. The expected cumulative velocities are much larger and do not appear to be quickly tending to below 1. Figure 4 shows how the distribution of minimized velocities after an observation changes as the number of iterations is increased. The effect of increasing the number of iterations is clearly to bring the distribution of expected instantaneous minimized velocities below 1.

In the case of Figures 2 through 4, p_d and p_r are both taken to be $1/2$. Figure 4 shows how the distribution of the expected minimized velocity of one PP takes the form of a Poisson distribution and bears similarities to the Maxwell–Boltzmann distribution of speeds in an idealized gaseous substance.

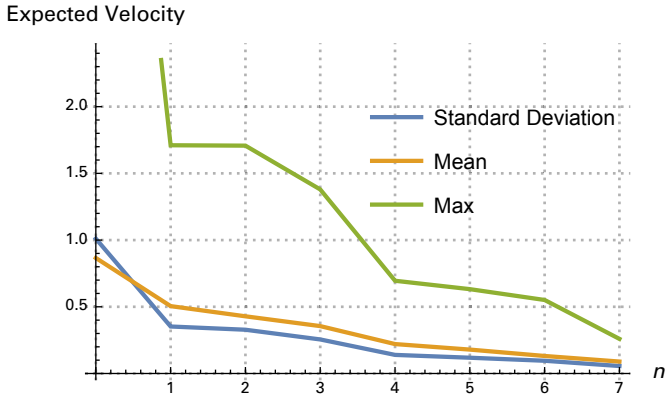

Figure 2. Here the mean, standard deviation and maximum value of the distribution of the expected minimized velocity of one of the PPs within a system embedded in $\mathbb{R}^3$ are shown, as the number of sample microstates $2^n \times 10$ increases. The measurements of velocity are taken in the TS after an observation with $\Delta x = 20$ is performed on the system.

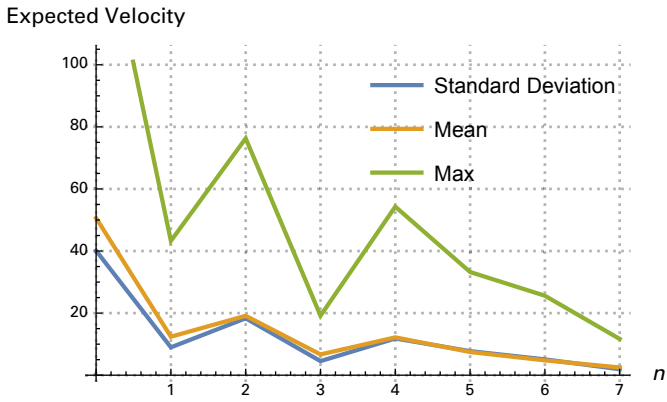

Figure 3. Here the mean, standard deviation and maximum value of the distribution of the expected cumulative velocity of one of the PPs within a system embedded in $\mathbb{R}^3$ are shown, as the number of sample microstates $2^n \times 10$ increases. The measurements of velocity are taken in the TS after an observation $\Delta x = 20$ is performed on the system.

In Figures 5 and 6, $1+1$-dimensional evolutions of one PP within the embedded system in $\mathbb{R}$ are shown. The straight red lines represent light cones of gradient 1 defined in $\mathbb{R}^n$ that begin once the PP has been observed. The gray lines represent the points in time of each observation (macrostate collapsing to a single microstate). The yellow

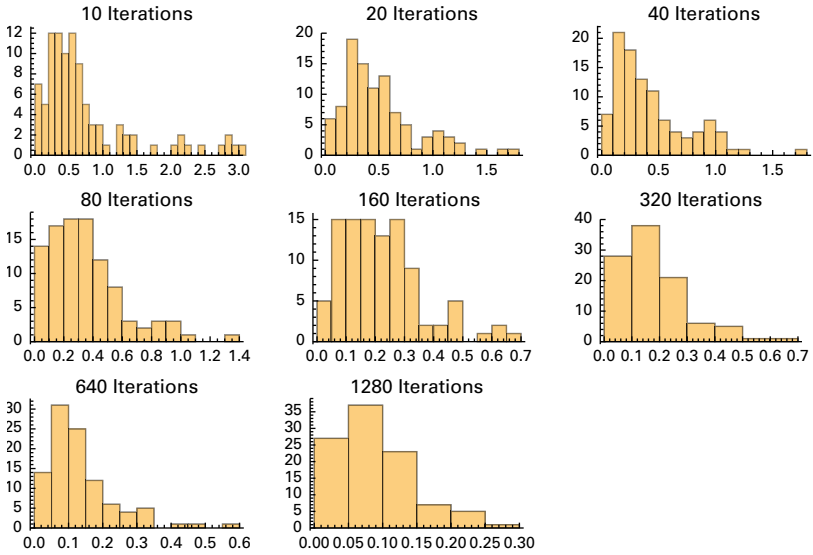

Figure 4. Histograms showing the distribution of the expected minimized velocity of a PP the TS after observation. These histograms correspond to a sample size of 100 microstates.

and blue lines show the evolution of the expected minimized and cumulative velocities, respectively. As can be seen clearly in Figure 5, the cumulative velocity has oscillatory motion about the stress minimum. However, in Figure 5(a) the path of the particle moves away from the stress minimum; this is because to increase the speed of the simulation, $\tilde{X}_t(\tilde{X}_{t-1})$ was used as opposed to $\tilde{X}_t(X_t)$. What this means is that there are multiple local minima. With a superluminal velocity, it is likely to be possible to jump between any two of these minima. It may also be possible for a particle oscillating about one local minimum, under macrostate collapse due to observation, to appear in a different minimum. This is similar to the effects of quantum tunneling or action at a distance of a spatially separated single-particle wavefunction.

Figure 5 provides evidence of how the overall expectation value of the stress-minimized location $\tilde{X}_t$ is constrained by the light cone dynamics. However, some of the microstate paths do move outside of the light cone temporarily. This is likely due to two main reasons. First, as shown in Figure 4, as the number of iterations of the stress-minimization algorithm is increased, the values for the velocity are brought to below one, so there may not have been enough iterations on this run. Second, each yellow dot represents a microstate, which

experiences temporary fluctuations in its state that would be evened out with both time and sample averaging (this could have some comparability to the quantum mechanical uncertainty principle). This means that when the light cone dynamics are violated by one of these microstates outside of the light cone being observed, as in Figure 6, the motion then moves back into the light cone only a few TSs later. The paths tend back into the light cone; this behavior is observed in all further observations of this kind. Figure 7 shows how as the probability of duplication and reduction is changed in favor of a greater rate of duplication, the average velocity of the PP is increased, but is very clearly constrained to the gradient of the light cone.

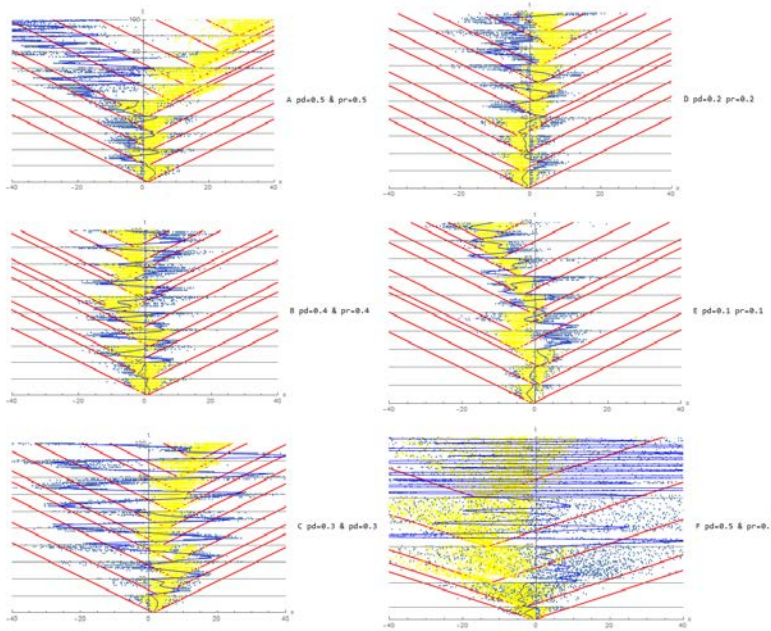

Figure 5. These six figures show various evolutions of the minimized and cumulative velocities of one PP in 1 + 1-dimensional spacetime diagrams. The system consists of three PPs, with the probabilities for the actions between the PP whose position is measured and the other two PPs given to the right of each evolution. After each observation, 100 microstate paths are followed; these are implemented using a Monte Carlo loop. Yellow points represent the locations of the stress minimum, and blue points represent the positions corresponding to the particle's cumulative velocity.

https://doi.org/10.25088/ComplexSystems.27.2.127

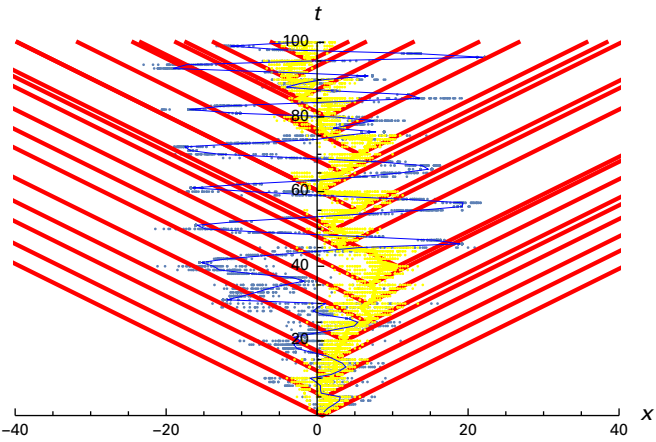

Figure 6. Evolution of a $1+1$-dimensional system where a small timescale light cone violation is observed.

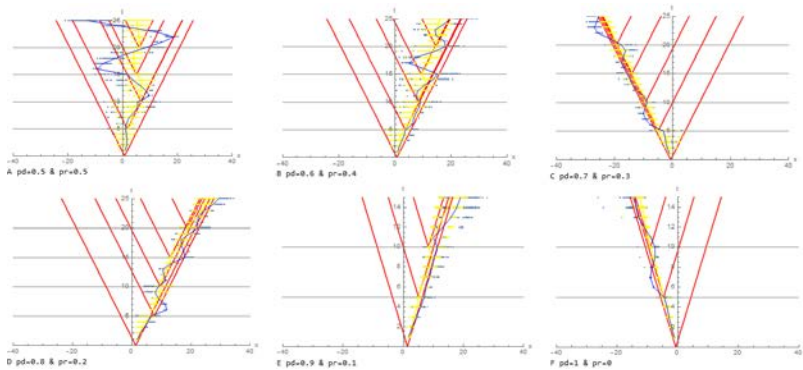

Figure 7. These six figures are defined in the same way as in Figure 6. The difference is that the ratio between the probability of duplication and reduction is changed to favor duplication. Here you can see how the expected minimum velocity and cumulative velocity merge toward the light cone limit. This behavior implies an emergent intrinsic limit on the particle's velocity.

Here there is a system that has a minimum stress location that obeys light cone dynamics (besides for specifically observed microstates at the very small timescales when observed). This is represented by the yellow in the light cone spacetime diagrams. It also has a position x_{it} that oscillates about the local stress minimum $\tilde{x}_{it}$ with a cumulative velocity. This is represented by the blue in the light cone spacetime diagrams. This may provide the potential to exhibit nonlocal action at a distance dynamics that, since it is fixed to oscillate

about the local stress minimum, still obeys fundamental relativistic principles. This behavior is emergent from the fundamental rules and structure of the system.

4. Discussion and Comparisons

This investigation is presented to show the preliminary evidence for the emergence of compatible relativistic and quantum behavior for this specific discrete network. The system implemented here is still incomplete, as it does not account for PP splitting and merging, multi-IEs and IE cloning [1]. Interaction edge classes were used in setting up the systems in Figures 5 through 7, but larger-scale interaction dynamics were not investigated in detail. There are a number of physical comparisons that will now be outlined in this section.

4.1 Mass

First, in [1] mass is defined within the system as directly related to the number of PPs local to a region. So particles of different masses can be defined as *clouds* of PPs whose rate of splitting is equal to their rate of merging, and so the number of PPs in a localized region remains constant. This means that if the stress minimum of a single PP obeys light cone dynamics, then it is true for all massive particles in the system, as the positions in space of massive clusters are defined as the vector average of the locations of PPs within the cluster.

Second, information propagates through all space, and therefore it is possible to define an information density of space. In [5] Verlinde argues that entropy change is proportional to mass by being able to split particles into subparticles; this is consistent with the notion of mass being defined by the number of constituent PPs within a localized space. He also argues that space is a storage space for information whose entropic dynamics in closed screens around particles with mass produce Newton's laws and Einstein gravity as an emergent entropic force. The density of information in this information-propagating graph is proportional to the area, and if we consider a screen around each particle, there is an emergent region (the updated state graph) and a hidden side (the hidden microstate). This theory has been validated further in [6].

Third, the greater the mass of a cluster, the greater the number of IEs incident on the enclosed PPs comprising the mass of the cluster. This is likely to have an effect on the frequency of the oscillation of the cluster due to an increased stress on the cluster, as the stress is proportional to the number of IEs incident in a region. This would result in particles of higher mass having higher frequencies; however, it

https://doi.org/10.25088/ComplexSystems.27.2.127

would be necessary to scale the system to the point where the stress on the region is vastly smaller than the total stress in the system. If splitting and merging were implemented in this system, it would further increase the number of multi-IEs incident on the cluster and so further increase the stress and therefore the frequency.

4.2 Internal Particle Spin

This model treats all massive particles as clusters of PPs, with some finite radius. This means that these clusters may contain internal angular momentum. If a magnetic force is exerted on particles in the system with charge, then the angular momentum of the PPs around the mean position of PPs of the cluster could have the effect of exerting a force on the PPs. This observation would be confined to particles with mass; massless bosons would not contain spin, as they are not constituted of PPs, besides a single PP that would seem to also have zero internal angular momentum, as it does not have any spatial extent. Spins would also sum, so long as they were in a local region of space. Since cumulative velocities of PPs are conserved over velocity transformations, action at a distance as described in this paper would not affect the spin of these particles. Further to this, since the velocities are superluminal, then the magnetic moment of particles has the potential to be accounted for this way. Further investigations into the spin of particle clusters in this system have been done and have shown that the total internal angular momentum of the PP clusters is independent from their mass, and that the spins appear to tend to well-defined equilibrium values. These results will be released in a later paper.

4.3 Coordinate Frame and Observation

Within this system, there is a definition of the frame of reference by which the state graph is embedded into $\mathbb{R}^n$ by the orientation vertex set [1]. This set can be changed to any set to define the new coordinate frame, which can be done via a basis transformation. Only PPs may be at the center of a coordinate frame, since they are the "observers." The information propagation speed is independent of the relative velocity of the centralized PP. The entire state of the system is updated at the centralized PP, much like the concept that all possibilities do not exist until they are observed. Observation of the particles' locations in $\mathbb{R}^n$ collapses the microstate ensemble to a smaller ensemble defined by an uncertainty. Observation, or collapse of the system into a smaller set of microstates, has the effect of inducing inhomogeneity in the evolution of the system, resulting in the formation of complex structures, depending on the definition of the observation.

4.4 Information and Energy Transfer

Energy within this system is defined as the rate of actions observed by the centralized PP. It is not created or destroyed in the propagation mechanism, and when it is finally incident on the centralized PP, it updates the state of the entire system, changing the stress distribution and velocities. Much like massless bosons transferring information at light speed, actions that occur within the system are propagated at an average velocity of 1 SE per TS, which scales to the speed of light if 1 is scaled to the plank length and that is taken to be the ultraviolet cutoff.

4.5 Interactions and Emergence of Complex Structures

This is an area with a lot of potential for further research. The implementation of IE classes with different values for p_d and p_r may provide a framework for complex interactions. Particles of different masses can be classified by splitting and merging clouds of PPs, and the interaction between these clouds can be governed by defined IEs that are cloned and brought into multi-IEs. These IE classes can be of three main types, $p_d < p_r$, $p_d = p_r$ and $p_d > p_r$. The first is likely to be the interaction that governs particle masses, the second is likely to behave elastically, much like the strong force, and the third could count for some form of repulsion or spatial expansion. Large scales of these systems would have interesting dynamics and likely complex stable structures emerging. Splitting, while in some cases affecting the particle's mass, may result in behavior that is comparable to weak decay and high energy particle interactions. This may be when a split creates an IE of a different class and a PP cloud is separated into two. These are all areas for future study. Some small-scale dynamical evolutions of this system can be seen at the following URLs: https://youtu.be/EKpzZymNGVg, https://youtu.be/yjFdHpJlsp4 and https://youtu.be/8oQVaJwJVUo. These visualizations show the evolution of a 4 PP system.

4.6 Entanglement and Quantum Tunneling

There are two classes of nonlocal entanglement dynamics emerging from this system. The first is the ability for a particle to move superluminally between local minima. This corresponds to the case of a single particle that has had its wavefunction separated in space, giving the appearance of having moved non-relativistically when an observation is made. This behavior can also be affiliated with a form of quantum tunneling, the ability for a particle to appear over an energy barrier simply due to the fact that its position probability amplitude is nonzero on the other side of the potential barrier. The second class results from the fact that this system uses two metrics, one for the

state graph G, E_t, and one for the configuration in $\mathbb{R}^n$, X_t. External forces on particles may make their distance in $\mathbb{R}^n$ be much greater than their distance in the graph G. If there are interactions through G that are independent of or minimally affected by X_t, then there is a possibility for these to take effect even if the two particles are at a great distance from each other in $\mathbb{R}^n$.

5. Conclusion

The results from this paper are still somewhat qualitative and preliminary; however, the aim is to explain the rules of the system and demonstrate both its simplicity and nontriviality in the context of physical compatibility. The hope is that other researchers will see the potential in this system and others like it and help in scaling up the simulations. Further experiments are to be done on this system and similar systems. These include testing for length contraction and time dilation, uncertainty principle, weak interactions (further investigations into point particle (PP) splitting and localized interaction edge (IE) action probabilities), particle masses (system stress and oscillations), particle spin, and thermodynamic and mechanical comparisons, as well as many others. Some of these experiments have already been implemented and research is underway, although issues regarding how you scale a system like this efficiently do need to be addressed, as well as how to implement all aspects of the system simultaneously. This is a great computational challenge; however, observing the behavior of such discrete dynamic physically comparable systems may give us some insight into the underlying mechanisms that govern the behaviors of real physical systems.

References

[1] T. L. Wood, "Emergence of Massive Equilibrium States from Fully Connected Stochastic Substitution Systems," *Journal of Cellular Automata*, **12**(3–4), 2017 pp. 189–208.

[2] D. Rideout and P. Wallden, "Emergence of Spatial Structure from Causal Sets," *Journal of Physics: Conference Series*, **174**(1), 2009 012017. doi:10.1088/1742-6596/174/1/012017.

[3] F. Markopoulou, "New Directions in Background Independent Quantum Gravity," *Approaches to Quantum Gravity: Toward a New Understanding of Space, Time and Matter* (D. Oriti, ed.), New York: Cambridge University Press, 2009 pp. 129–149. doi:10.1017/CBO9780511575549.010.

[4] M. Van Raamsdonk, "Building Up Space–Time with Quantum Entanglement," *International Journal of Modern Physics D*, **19**(14), 2010 pp. 2429–2435. doi:10.1142/S0218271810018529.

[5] E. Verlinde, "On the Origin of Gravity and the Laws of Newton," *Journal of High Energy Physics*, **2011**(4), 2011 p. 29. doi:10.1007/JHEP04(2011)029.

[6] E. P. Verlinde, "Emergent Gravity and the Dark Universe," *SciPost Physics*, **2**(3) 2017 016. doi:10.21468/SciPostPhys.2.3.016.

[7] P. Jizba and F. Scardigli, "Cooperative Dynamical Processes: The Emergence of Relativistic Quantum Theory," *Journal of Physics: Conference Series*, **504**(1), 2014 012012. stacks.iop.org/1742-6596/504/i=1/a=012012.

[8] V. Sahakian, Y. Tawabutr and C. Yan, "Emergent Spacetime and Quantum Entanglement in Matrix Theory," *Journal of High Energy Physics*, **2017**(8) 140. doi:10.1007/JHEP08(2017)140.

[9] J. Henson, "The Causal Set Approach to Quantum Gravity," *Approaches to Quantum Gravity: Toward a New Understanding of Space, Time and Matter* (D. Oriti, ed.), New York: Cambridge University Press, 2009 pp. 393–413. doi:10.1017/CBO9780511575549.025.

[10] D. D. Reid, "Introduction to Causal Sets: An Alternate View of Spacetime Structure." arxiv.org/abs/gr-qc/9909075.

[11] J. Eakins and G. Jaroszkiewicz, "The Origin of Causal Set Structure in the Quantum Universe." arxiv.org/abs/gr-qc/0301117.

[12] J. Ambjorn, J. Jurkiewicz and R. Loll, "Causal Dynamical Triangulations and the Quest for Quantum Gravity." arxiv.org/abs/1004.0352.

[13] R. D. Sorkin, "Spacetime and Causal Sets," *Relativity and Gravitation: Classical and Quantum, Proceedings of the SILARG VII Conference*, Cocoyoc, Mexico, 1990 (J. C. D'Olivo, E. Nahmad-Achar, M. Rosenbaum, M. P. Ryan, L. F. Urrutia and F. Zertuche, eds.), Singapore: World Scientific, 1991 pp. 150–173. doi:10.1142/9789814538657.

[14] A. Ilachinski, *Cellular Automata: A Discrete Universe*, River Edge, NJ: World Scientific, 2001.

[15] S. Wolfram, *A New Kind of Science*, Champaign, IL: Wolfram Media, Inc., 2003.

[16] S. Lloyd, "The Universe as Quantum Computer," *A Computable Universe: Understanding and Exploring Nature As Computation* (H. Zenil, ed.), Hackensack, NJ: World Scientific, 2013.

[17] R. P. Feynman, "Simulating Physics with Computers," *International Journal of Theoretical Physics*, **21**(6–7), 1982 pp. 467–488. doi:10.1007/BF02650179.

[18] J. von Neumann, *The Theory of Self-Reproducing Automata* (A. W. Burks, ed.), Urbana, IL: University of Illinois Press, 1996.

[19] G. Grössing and A. Zeilinger, "Quantum Cellular Automata," *Complex Systems*, **2**(2), 1988 pp. 197–208. complex-systems.com/pdf/02-2-4.pdf.

[20] G. Hooft, "The Cellular Automaton Interpretation of Quantum Mechanics." arxiv.org/abs/1405.1548.

[21] G. M. D'Ariano, "Physics as Quantum Information Processing: Quantum Fields as Quantum Automata." arxiv.org/abs/1110.6725.

[22] G. M. D'Ariano and P. Perinotti, "Derivation of the Dirac Equation from Principles of Information Processing," *Physical Review A*, **90**(6), 2014 062106. doi:10.1103/PhysRevA.90.062106.

[23] A. Bisio, G. M. D'Ariano, P. Perinotti and A. Tosini, "Free Quantum Field Theory from Quantum Cellular Automata," *Foundations of Physics*, **45**(10), 2015 pp. 1137–1152. doi:10.1007/s10701-015-9934-1.

[24] G. M. D'Ariano and P. Perinotti, "Quantum Cellular Automata and Free Quantum Field Theory," *Frontiers of Physics*, **12**(1), 2017 120301. doi:10.1007/s11467-016-0616-z.

[25] M. Requardt, "Cellular Networks as Models for Planck-Scale Physics," *Journal of Physics A: Mathematical and General*, **31**(39), 1998 7997. stacks.iop.org/0305-4470/31/i=39/a=014.

[26] M. Requardt, "(Quantum) Spacetime as a Statistical Geometry of Lumps in Random Networks," *Classical and Quantum Gravity*, **17**(10), 2000 2029. stacks.iop.org/0264-9381/17/i=10/a=301.

[27] M. Requardt and S. Rastgoo, "The Structurally Dynamic Cellular Network and Quantum Graphity Approaches to Quantum Gravity and Quantum Geometry: A Review and Comparison," *Journal of Cellular Automata*, **10**(5–6), 2015 pp. 341–392.

[28] T. Konopka, F. Markopoulou and S. Severini, "Quantum Graphity: A Model of Emergent Locality," *Physical Review D*, **77**(10), 2008 104029. doi:10.1103/PhysRevD.77.104029.

[29] H. Vucetich, "Testing Lorentz Invariance Violation in Quantum Gravity Theories." arxiv.org/abs/gr-qc/0502093.

[30] A. Einstein, "Ist die Trägheit eines Körpers von seinem Energieinhalt abhängig?," *Annalen der Physik*, **323**(13), 1905 pp. 639–641. doi:10.1002/andp.19053231314.

[31] C. G. Timpson and H. R. Brown, "Entanglement and Relativity." arxiv.org/abs/quant-ph/0212140.

[32] A. Nahum, J. Ruhman and D. A. Huse, "Dynamics of Entanglement and Transport in 1D Systems with Quenched Randomness." arxiv.org/abs/1705.10364.